JMEPEG (2019) 28:4111–4119
https://doi.org/10.1007/s11665-019-04162-4

©ASM International
1059-9495/$19.00

Effect of Cobalt Content on Thermal, Mechanical, and Microstructural Properties of $Al_{0.4}FeCrNiCo_x$ (x = 0, 0.25, 0.5, 1.0 mol) High-Entropy Alloys

Saurav Kumar, Amar Patnaik, Ajaya Kumar Pradhan, and Vinod Kumar

(Submitted December 9, 2018; in revised form March 27, 2019; published online July 2, 2019)

$Al_{0.4}FeCrNiCo_x$ (x = 0, 0.25, 0.5, 1.0 mol) high-entropy alloys are developed by arc melting route to investigate the effect of cobalt content on thermal, mechanical, and microstructural properties. The phase, microstructure, and chemical composition are analyzed using x-ray diffraction, transmission electron microscope, and scanning electron microscope with attached energy-dispersive x-ray spectrometer. The obtained results have shown that the $Al_{0.4}FeCrNiCo_x$ (x = 0-0.5 mol) high-entropy alloys form a simple FCC + BCC-type solid solution and $Al_{0.4}FeCrNiCo_{x=1}$ HEA forms a single-phase FCC structure. The compressive yield strength, microhardness, and thermal conductivity are observed to decrease from 965.22 to 233.37 MPa, 253.6 to 155.6 HV, and from 4.87 to 2.674 W/mK, respectively, whereas the electrical resistivity is observed to increase from 150.30 to 273.74 μΩ-cm with the addition of cobalt from x = 0-1 mol. Differential scanning calorimetry analysis has indicated that the $Al_{0.4}FeCrNiCo_x$ (x = 0, 0.25, 0.5, 1.0 mol) high-entropy alloys are thermally stable up to 1000 °C.

Keywords DSC, hardness, high-entropy alloy, thermal conductivity

1. Introduction

High-entropy alloys (HEAs) are a relatively new class of materials design concept and have been observed to exhibit better properties than traditional alloys. This new alloy system was first reported by Yeh et al. (Ref 1). These HEAs consist of four or more elements, and each element is in equimolar or near equimolar concentration (Ref 2, 3). These HEAs are found to have, high-temperature stability (Ref 4, 5), good mechanical strength (Ref 6-11), better corrosion resistance (Ref 12-14), improved oxidation resistance (Ref 15, 16), better magnetic properties (Ref 17, 18), and superior wear resistance properties (Ref 19-22). Generally, these HEAs form a simple crystal structure, and it is due to the high entropy of mixing (Ref 23). Zhang et al. (Ref 24) have discovered a criterion which can predict the solid-solution formation ability of multi-component HEAs such as $\Omega > 1.1$, $\delta < 6.6\%$. And Guo et al. (Ref 25) have introduced another parameter called valence electron concentration (VEC) to predict the structural stability of HEAs, and according to this criterion, if VEC < 8.0, it favors the formation of only BCC structure, and if VEC ≥ 8, it favors only FCC structure and in between it forms FCC + BCC structure.

Among various HEA systems, the Al-Fe-Cr-Ni-Co HEA system has been investigated thoroughly and reported extensively. The equiatomic AlFeCrNiCo HEAs exhibit high corrosion resistance, good mechanical strength, and poor ductility (Ref 6, 26). Due to poor ductility and hence formability, it faces various challenges during rolling, forging, and other mechanical processing. In order to develop an alloy which fulfills the demands of different engineering problems, it should have the right combination of strength and ductility. The simplest way to achieve this objective is by changing the concentration of elements present in Al-Fe-Cr-Ni-Co HEA system. Aluminum has frequently been varied to tailor the mechanical properties of the Al-Fe-Cr-Ni-Co HEA system (Ref 27-29). Kao et al. (Ref 30) have reported that $Al_XFeCrNiCo$ (x = 0-2.0) HEAs only exhibit FCC phase and a hardness between 113 and 130 HV till the concentration of Al reaches 0.375. For Al concentration in between 0.5 and 0.75, a dual-phase (FCC + BCC) structure forms and the corresponding hardness is observed to vary between 159 and 388 HV. When Al concentration is in between 0.875 and 2.0, only a single BCC phase gets formed with the highest hardness value of 509 HV. Wani et al. (Ref 31) have altered the nickel concentration and have observed the formation of a mixed phase of FCC and BCC structure. Wang et al. (Ref 29) have varied the concentration of iron and nickel in the HEA and have observed the formation of a single FCC phase. Few studies are also available on the variation of the cobalt concentration which has summarized that as cobalt content increases; the phase structure transforms from BCC to FCC occur (Ref 32-35). Hence, from the above-mentioned findings, it may be concluded that the addition of cobalt in Al-Fe-Cr-Ni-Co HEA increases the ductility, while the addition of aluminum increases the strength of the HEA (Ref 30).

The present work aims to develop the $Al_{0.4}FeCrNiCo_x$ (x = 0, 0.25, 0.5, 1.0 mol) HEAs through arc melting route

Saurav Kumar and **Ajaya Kumar Pradhan**, Department of Metallurgical and Materials Engineering, MNIT, Jaipur 302017, India; **Amar Patnaik**, Department of Mechanical Engineering, MNIT, Jaipur 302017, India; and **Vinod Kumar**, Discipline of Metallurgy Engineering and Materials Science, IIT Indore, Indore 453552, India. Contact e-mails: apatnaik@mnit.ac.in and vkt@iiti.ac.in.

using cold-compacted pellet as raw material. Investigations are carried out to study the effect of cobalt content on thermal, mechanical, and microstructural properties of as-cast HEAs. Furthermore, thermodynamic criterion is also obtained to predict the crystal structure in $Al_{0.4}FeCrNiCo_x$ (x = 0, 0.25, 0.5, 1.0 mol) HEAs.

2. Materials and Methods

The bulk $Al_{0.4}FeCrNiCo_x$ (x = 0, 0.25, 0.5, 1.0 mol) HEAs ingot is prepared using cold-compacted pellets as the raw material in vacuum arc melting furnace as shown in Fig. 1(a). The cold compaction is carried out in a 12-mm-inner-diameter high-speed steel die using a load of 10 tons and employing a simple hydraulic press (Kimaya Engineers-15 Tones) at room temperature. Elemental powders of Al, Fe, Cr, Ni, Co (Loba Chemie, India) with purity more than 99.5% are used for the current research and are hand-mixed in appropriate proportion before compaction. The melting is carried out employing a protective atmosphere of argon and in a water-cooled copper mold. In order to obtain proper chemical homogeneity, the sample is melted several times. The final ingots are in the form of a near cylindrical shape with dimensions of (Ø 14 mm × 45 mm) and in the form of a circular button shape with dimension of (Ø 16 mm × 12 mm) as shown in Fig. 1(b) and (c), respectively. The crystal structure of the as-cast HEA is identified using X'Pert Pro Panalytical, x-ray diffractometer and employing Cu Kα (λ = 0.154059 nm) radiation. Transmission electron microscope (Tecnai 20, FEI) operated at 200 kV is used to confirm the formation of different phases. The microstructures of the different samples are observed using FE-SEM (Nova Nano 450SEM, FEI) after etching with aqua regia, and the corresponding chemical compositions are obtained using the attached energy-dispersive x-ray spectroscopy (EDS). The volume fraction calculation is carried out using image analysis software (ImageJ). The thermal stability of the as-cast HEAs is determined in the temperature range ambient (25 °C) to 1000 °C using a differential scanning calorimeter (Netzsch, DSC 404 F3) employing a heating rate of 10 K/min. The thermal conductivity of the HEA samples with dimensions of (Ø 16 mm × 2 mm) is measured at room temperature by hot disk method using a Hot Disk TPS 500 apparatus. The microhardness of the HEA samples is measured in a microhardness tester (VMHT, Walter-Uhl) using a load of 200 gf and applied for a dwell time of 15 s. For the compressive test, cylindrical specimens with dimensions of (Ø4 mm × 4 mm) are used, and the test is carried out at a loading rate of 0.5 mm/min in a (BISS UT 21). To avoid difficulty in writing $Al_{0.4}FeCrNiCo_{x=0}$, $Al_{0.4}FeCrNiCo_{x=0.25}$, $Al_{0.4}FeCrNiCo_{x=0.5}$, and $Al_{0.4}FeCrNiCo_{x=1}$, HEAs are denoted as Co = 0, Co = 0.25, Co = 0.5, Co = 1 HEA, respectively, in the text afterward.

3. Results and Discussion

3.1 Microstructure and Phase Analysis of $Al_{0.4}FeCrNiCo_x$ (x = 0, 0.25, 0.5, 1.0 mol) HEA

Figure 2 shows the x-ray diffraction pattern of as-cast $Al_{0.4}FeCrNiCo_x$ (x = 0, 0.25, 0.5, 1.0 mol) HEAs. The peak reflections of $Al_{0.4}FeCrNiCo_x$ (x = 0-0.5 mol) HEAs have a mixed phase of FCC and BCC structure. However, in the case of Co = 1 HEA, it has only the FCC phase. The lattice constants and the volume fractions of BCC and FCC are calculated from the x-ray diffraction and SEM micrograph and are listed in Table 1. The calculated values of lattice constants for both the phases are in close agreement with those available in the literature (Ref 28, 30, 36). As the concentration of cobalt increases from x = 0-0.5 mol, the BCC peaks start vanishing and they completely disappear at x = 1.0 mol. The volume fraction of the FCC phase increases from 83.5 to 98.5%, and that of the BCC phase decreases from 16.5 to 1.5% for the increase in cobalt content from x = 0 to 0.5 mol. It is also observed from the XRD graph (Fig. 2) that the peak intensity of (111) plane is gradually increasing with the increase in the amount of cobalt. From the above discussion, it may be concluded that the cobalt is an FCC phase former in $Al_{0.4}FeCrNiCo_x$ (x = 0, 0.25, 0.5, 1.0 mol) HEAs.

Figure 3 shows the BSE–SEM micrograph of as-cast HEAs with varying cobalt content, and it is observed that the Co = 0, Co = 0.25, Co = 0.5 HEAs form a mixed phase of FCC and BCC structure and the two regions are designated as zone A and zone B, respectively. The microstructure for Co = 1 HEA shows only a single region of FCC phase. The compositional analysis of different regions obtained from EDS analysis is listed in Table 2. The EDS results show that the regions poor in Al form FCC structure as reported in the previous literature (Ref 35, 37), whereas the regions rich in Al and (Fe, Cr) form BCC structure and the region rich in Al and Ni form Al-Ni phases or B2 phase.

The reason behind the formation of Al-Ni phase is the larger negative enthalpy of mixing between Al and Ni (− 22 kJ/mol) than the other atomic pairs present in the alloy system, and this inference is consistent with the previous studies (Ref 7, 30). As

Fig. 1 (a) Cold-compacted pellet, (b) cylindrical shape, and (c) button shape of as-cast HEA samples

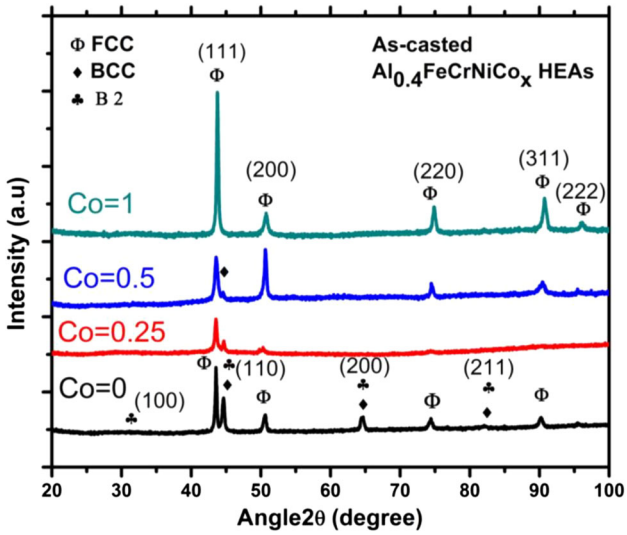

Fig. 2 X-ray diffraction pattern of as-cast $Al_{0.4}FeCrNiCo_x$ (x = 0, 0.25, 0.5, 1.0 mol) HEAs

Table 1 Lattice parameter and volume fractions of as-cast $Al_{0.4}FeCrNiCo_x$ (x = 0, 0.25, 0.5, 1.0 mol) HEAs

	Lattice parameter, Å		Volume fraction, %	
HEAs	FCC phase	BCC phase	FCC phase	BCC phase
Co = 0	3.5949	2.8686	83.5	16.5
Co = 0.25	3.5959	2.8674	93.0	7.0
Co = 0.5	3.5939	2.8700	98.5	1.5
Co = 1	3.5787	…	100	0

the cobalt concentration increases from Co = 0.25 to Co = 0.5 HEA, zone 'B' drastically decreases and uniform homogeneous mixture of Fe, Cr, Ni, and Co forms. It has been confirmed from the STEM results of the HEAs (Fig. 5). The solid solution of Co, Cr, Fe, and Ni is having FCC crystal structure as reported in previous studies (Ref 38).

Figure 4 shows the TEM bright-field image, dark-field image, and SAED pattern of as-cast $Al_{0.4}FeCrNiCo_x$ (x = 0, 0.25, 0.5 mol) HEAs. In the bright-field TEM image, all the phases cannot be easily distinguished from the image contrast. Chemical compositions (at.%) of the phases present in as-cast HEAs are identified by the EDS (Fig. 5). The results indicate that both darker and lighter portion have uniform regions consisting of Co, Cr, Fe, and Ni.

3.2 Thermal Analysis of $Al_{0.4}FeCrNiCo_x$ (x = 0, 0.25, 0.5, 1.0 mol) HEAs

The DSC curve as shown in Fig. 6 indicates that there is no sign of any phase changes up to 1000 °C in the HEA samples, as the DSC curve does not show the presence of any significant endothermic/exothermic peaks. This confirms that the $Al_{0.4}FeCrNiCo_x$ (x = 0, 0.25, 0.5, 1.0 mol) HEAs are thermally stable up to 1000 °C.

3.3 Thermal Conductivity of $Al_{0.4}FeCrNiCo_x$ (x = 0, 0.25, 0.5, 1.0 mol) HEAs

Figure 7 shows the variation of thermal conductivity of $Al_{0.4}FeCrNiCo_x$ (x = 0, 0.25, 0.5, 1.0 mol) HEAs. The reported thermal conductivity is the average of five readings of different samples of the same composition. From Fig. 7, it is observed that with the increase in cobalt content from x = 0-1.0 mol, the thermal conductivity decreases from 4.87 to 2.674 W/mK. It is because the aluminum content decreases as listed in Table 2 with the addition of cobalt content from x = 0 to 1.0 mol, and the BCC phase decreases from 16.5 to 0% (Table 1). It may be noted that the thermal conductivity of aluminum is highest among all the other elements as listed in Table 4. Similar results are also reported in previous studies (Ref 39, 40). As the cobalt content increases, the volume fraction of BCC phase decreases, and it results in a decrease in thermal conductivity. It may also be noted that the BCC structure is a more open structure than the FCC structure and possesses higher phonon velocity than FCC structure.

The phonon velocity is calculated from Eq 1 (Ref 39).

$$\text{phonon velocity} = \left(\frac{E}{\rho}\right)^{1/2} \quad \text{(Eq 1)}$$

where E is the Young's modulus (in GPa) and ρ is the density (in g/cm^3). It is observed that the phonon velocity decreases from 919.66 to 775.24 m/s with an increase in cobalt content from x = 0-1.0 mol and therefore thermal conductivity decreases from 4.87 to 2.674 W/mK. According to Wiedemann–Franz law (Ref 39), the ratio of thermal conductivity (k) to electrical conductivity (σ) of a metal is directly proportional to temperature, and it is represented by Eq 2.

$$\frac{k}{\sigma} = LT \quad \text{(Eq 2)}$$

where L is the proportionality constant known as the Lorenz number. The value of L is 2.44×10^{-8} WΩK^{-2}, and T is the temperature in Kelvin. From Eq 2, the electrical conductivity of $Al_{0.4}FeCrNiCo_x$ (x = 0, 0.25, 0.5, 1.0 mol) HEAs is observed to decrease from 6.65×10^5 to 3.65×10^5 m$^{-1}\Omega^{-1}$. The electrical resistivity (ρ) is defined as the reciprocal of the electrical conductivity and is given by Eq 3.

$$\rho = \frac{1}{\sigma} \quad \text{(Eq 3)}$$

Based upon the above equation, the electrical resistivity of the $Al_{0.4}FeCrNiCo_x$ (x = 0, 0.25, 0.5, 1.0 mol) HEAs is observed to vary from 150.30 to 273.74 μΩ-cm which is consistent with the values as reported in the previous literature (Ref 39, 40). It can be concluded that the amount of phases present and the chemical composition of these phases are the key parameters to decide the thermal conductivity and electrical conductivity of HEAs.

3.4 Mechanical Properties

The microhardness values of as-cast $Al_{0.4}FeCrNiCo_x$ (x = 0, 0.25, 0.5, 1.0 mol) HEAs are listed in Table 3. It is observed that as cobalt content increases, the microhardness decreases from 253.6 to 155.6 HV.

The engineering stress–strain curve of as-cast $Al_{0.4}FeCrNiCo_x$ (x = 0, 0.25, 0.5, 1.0 mol) HEAs, under compression loading at room temperature, is shown in Fig. 8.

The compressive yield strength (σ_y) and plastic strain (ε_p) of $Al_{0.4}FeCrNiCo_x$ (x = 0, 0.25, 0.5, 1.0 mol) HEAs are listed in Table 3. It is noted that the compressive yield strength

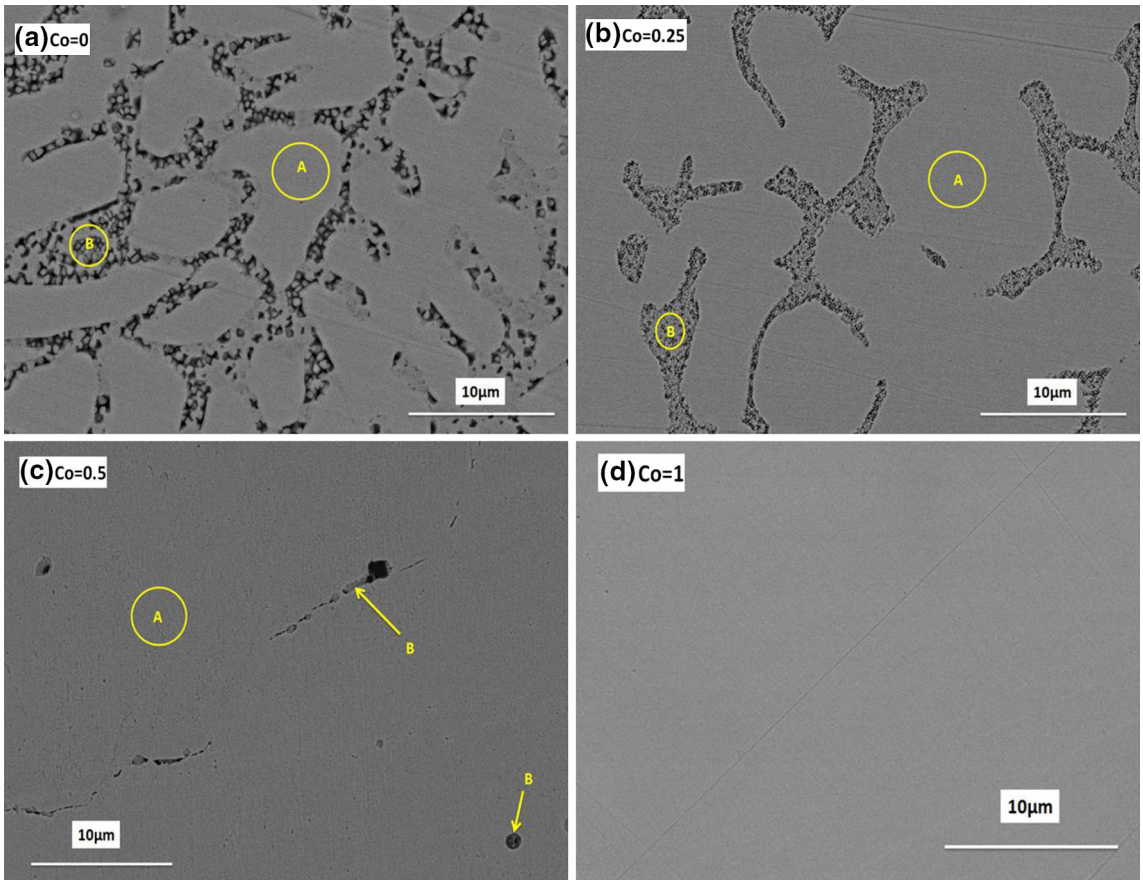

Fig. 3 BSE–SEM micrograph of as-cast (a) Co = 0 HEA, (b) Co = 0.25 HEA, (c) Co = 0.5 HEA, and (d) Co = 1 HEA

Table 2 EDS results (in at.%) of $Al_{0.4}FeCrNiCo_x$ (x = 0, 0.25, 0.5, 1.0 mol) HEAs

HEAs	Region	Al, at.%	Fe, at.%	Cr, at.%	Ni, at.%	Co, at.%
Co = 0	Overall	13.78	27.67	28.14	30.41	...
	A (FCC)	10.60	30.24	27.82	31.34	...
	B (BCC)	21.56	22.01	26.81	29.62	...
Co = 0.25	Overall	10.23	27.96	28.37	26.50	6.94
	A (FCC)	9.96	28.18	28.09	26.18	7.59
	B (BCC)	19.0	20.87	26.23	27.88	6.02
Co = 0.5	Overall	7.96	27.02	25.80	25.79	13.49
	A (FCC)	8.06	25.59	26.21	26.79	13.35
	B (BCC)	17.50	16.06	42.16	15.82	8.46
Co = 1	Overall	6.57	23.68	22.01	23.71	24.03

decreases from 965.22 to 233.37 MPa for the rise in cobalt content from x = 0-1.0 mol. A maximum plastic strain of 81% is observed in the case of $Al_{0.4}FeCrNiCo_{x=1}$ HEA and sample remains unfractured at the end of the experiment. There are two potential reasons for the decrease in compressive yield strength and microhardness values in case of $Al_{0.4}FeCrNiCo_x$ (x = 0, 0.25, 0.5, 1.0 mol) HEAs: (1) the vol.% of BCC phase varies from 16.5 to 0% as a result of addition of cobalt which plays a key role, and (2) the amount of stacking faulty present in FCC phase and its corresponding energy change their mechanical characteristics, responsible for lowering its mechanical strength.

3.5 Thermodynamic Parameters

In conventional alloys, the solid solution only forms when it satisfies the condition of the Hume–Rothery rule such as atomic size difference (less than 15%), and similar crystal structure, valency, and electronegativity (Ref 3). In the case of HEAs, the formation of simple solid solution like FCC, BCC, or mixed crystal structure of FCC + BCC (Ref 41) can be predicted, when it satisfies certain thermodynamic criteria as discussed below.

$$\Delta H_{\text{mix}} = \sum_{i=1, i\neq j}^{n} \Omega_{ij} C_i C_j \qquad \text{(Eq 4)}$$

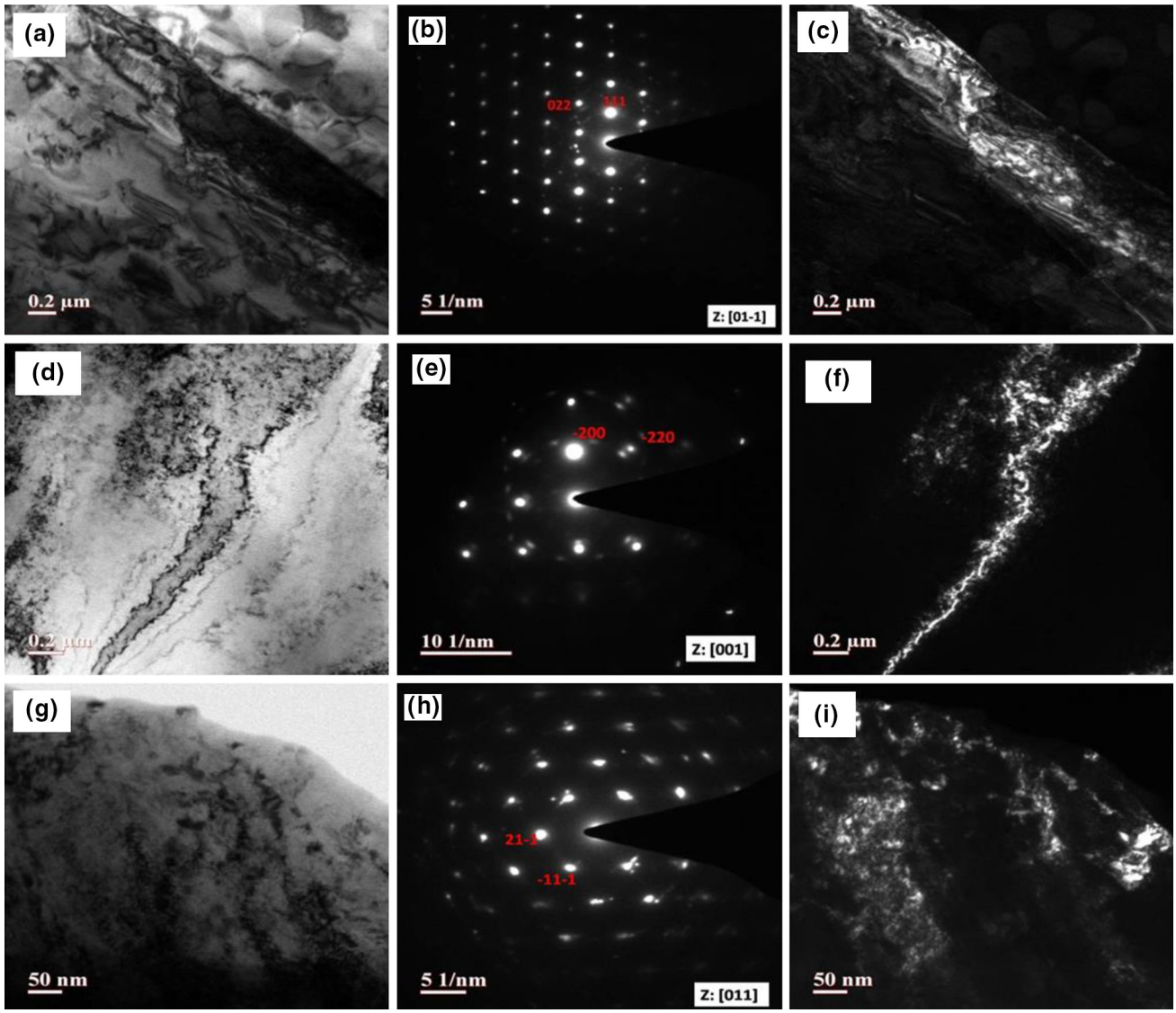

Fig. 4 TEM bright-field image, corresponding SAED pattern and dark-field image of as-cast (a-c) Co = 0 HEA, (d-f) Co = 0.25 HEA, and (g-i) Co = 0.5 HEA, respectively

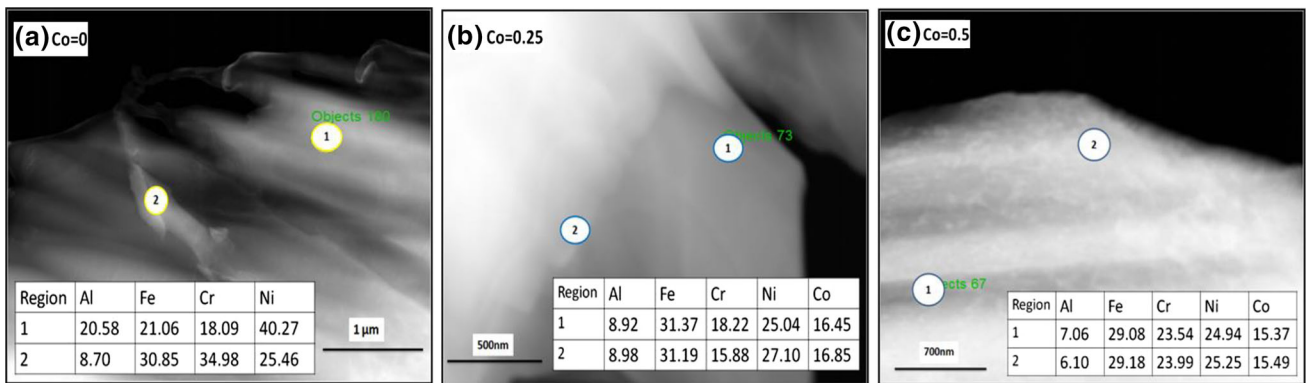

Region	Al	Fe	Cr	Ni
1	20.58	21.06	18.09	40.27
2	8.70	30.85	34.98	25.46

Region	Al	Fe	Cr	Ni	Co
1	8.92	31.37	18.22	25.04	16.45
2	8.98	31.19	15.88	27.10	16.85

Region	Al	Fe	Cr	Ni	Co
1	7.06	29.08	23.54	24.94	15.37
2	6.10	29.18	23.99	25.25	15.49

Fig. 5 STEM image and EDS analysis results of as-cast (a) Co = 0, (b) Co = 0.25, and (c) Co = 0.5 HEAs

$$\Delta S_{\text{mix}} = -R\sum_{i=1}^{n} C_i \ln C_i \quad \text{(Eq 5)}$$

$$\delta = 100\sqrt{\sum_{i=1}^{n} C_i\left(1-\frac{r_i}{\bar{r}}\right)^2} \quad \text{(Eq 6)}$$

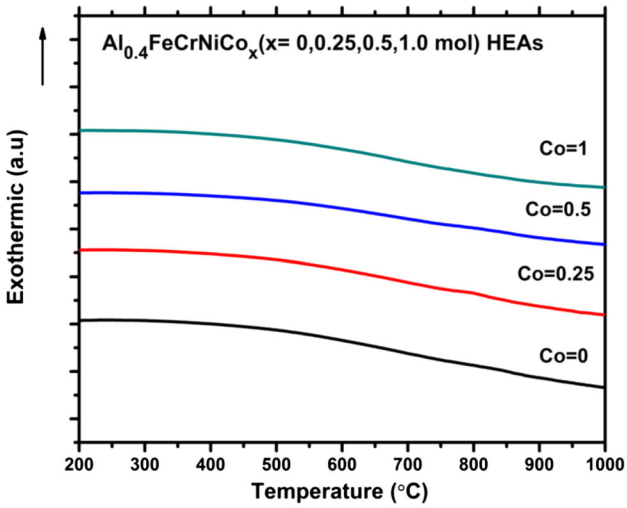

Fig. 6 DSC curves for as-cast $Al_{0.4}FeCrNiCo_x$ (x = 0, 0.25, 0.5, 1.0 mol) HEAs

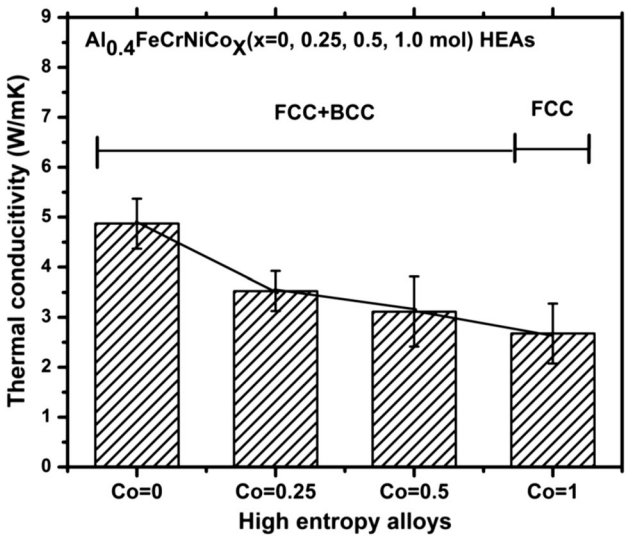

Fig. 7 Thermal conductivity of $Al_{0.4}FeCrNiCo_x$ (x = 0, 0.25, 0.5, 1.0 mol) HEAs

$$\Omega = \frac{T_m \Delta S_{\text{mix}}}{I\Delta H_{\text{mix}} I} \quad \text{(Eq 7)}$$

$$\text{VEC} = \sum_{i=1}^{n} C_i(\text{VEC})_i \quad \text{(Eq 8)}$$

$$\Delta X = \sqrt{\sum_{i=1}^{N} C_i\left(X_i - X_{\text{avg}}\right)^2} \quad \text{(Eq 9)}$$

$$T_{m,\text{th}} = \sum_{i=1}^{n} C_i(T_m)_i \quad \text{(Eq 10)}$$

where ΔH_{mix} is the enthalpy of mixing, ΔS_{mix} is the entropy of mixing of a multi-component alloy system, δ is the atomic size mismatch, and Ω is the thermodynamic parameter used to predict the solid-solution formation. VEC is the valence electron concentration which helps in predicting the formation of FCC, BCC, and dual-phase (FCC + BCC)-type solid solution, ΔX is the electronegativity difference which helps in understanding the phase stability, and $T_{m,\text{th}}$ is the theoretical melting point of multi-component alloys. The values of individual elements are taken from the previous literature (Ref 42-45) and are listed in Tables 4 and 5.

Figure 9(a) and (b) and Fig. 10 show the variation of the thermodynamic parameter with cobalt content. From Fig. 9(a),

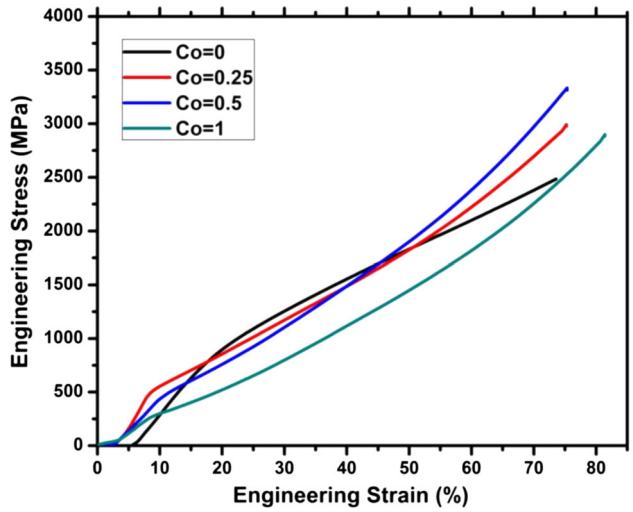

Fig. 8 Engineering stress–strain curves of as-cast, $Al_{0.4}FeCrNiCo_x$ (x = 0, 0.25, 0.5, 1.0 mol) HEAs under compression test

Table 3 Mechanical properties of Al0.4FeCrNiCo$_x$ (x = 0, 0.25, 0.5, 1.0) HEAs at room temperature

HEAs	Yield strength (σ_y) in MPa	Plastic strain, ε_p %	Microhardness, HV	Volume fraction of BCC, %
Co = 0	965.22	73.31	253.6	16.5
Co = 0.25	521.91	75.08	205.4	7.0
Co = 0.5	464.37	75.58	189.3	1.5
Co = 1	233.37	81.32	155.6	0

it can be seen that valence electron concentration (VEC) increases from 7.4 to 7.8 with the addition of cobalt content from $x = 0$ mol to $x = 1.0$ mol which indicates the transformation of FCC + BCC-type structure to only FCC-type structure. Figure 9(b) represents the variation of enthalpy of mixing (ΔH) and entropy of mixing (ΔS) with cobalt content. From the figure, it is observed that ΔS increases from 11.0 to 13.0 J/K^{-1}mol^{-1} and ΔH varies from − 9.4 to − 8.2 kJ/mol with the addition of cobalt from $x = 0$ to $x = 1.0$ mol. Figure 10 shows the variation of thermodynamic parameter Ω and δ%, with cobalt content and from the figure, it may be observed that Ω increases from 1.177 to 2.38 and the atomic radius mismatch (δ%) decreases from 0.047 to 0.041. From Eq 7, if $\Omega > 1$, then $T\Delta S$ is more than that of ΔH_{mix} and in this case, the HEA will form a simple solid solution. The ΔX value is observed to vary from 0.115 to 0.110, which satisfy the condition of no topologically close-packed (TCP) phase formation, i.e., $\Delta X < 0.117$ (Ref 46). Theoretical melting temperatures ($T_{m,Th}$) of the HEAs are estimated from Eq 10 and are observed that there is slight change in $T_{m,Th}$ (from 1509.06 to 1506.16 °C) with the addition of cobalt from $x = 0$ to $x = 1.0$ mol.

It is noted that the calculated values of thermodynamic parameter satisfy the criteria put forward by Zhang. et al. (Ref 43) and Guo. et al. (Ref 42, 44) for solid-solution formation, i.e., for $11 < \Delta S_{mix} < 19.5$ J/(K mol), $-22 < \Delta H_{mix} < 7$ kJ/mol, and $0 < \delta < 8.5$. If VEC < 6.87, then only BCC structure will form, if 6.87 < VEC < 8, then both BCC + FCC structure will form, and if VEC > 8, only FCC phase will form.

Table 4 Atomic size, melting point, thermal conductivity, crystal structure, lattice parameter, Pauling electronegativity, and VEC of an individual element (Ref 42-44)

Elements	Al	Fe	Cr	Ni	Co
Atomic size, Å	1.432	1.241	1.249	1.246	1.251
Melting temperature, T_m °C	660.3	1538	1875	1455	1495
Thermal conductivity, W/mK	237	80.2	93.7	83	100
Crystal structure	FCC	BCC	BCC	FCC	HCP
Lattice parameter, Å	4.049	2.866	2.884	3.524	3.545
Pauling electronegativity	1.61	1.83	1.66	1.91	1.88
VEC	3	8	6	10	9

Table 5 The mixing enthalpy (kJ/mol) of atomic pairs possible in $Al_{0.4}FeCrNiCo_x$ HEA system

Element	Al	Cr	Fe	Co	Ni
Al	0	− 10	− 11	− 19	− 22
Cr		0	− 1	− 4	− 7
Fe			0	− 1	− 2
Co				0	0
Ni					0

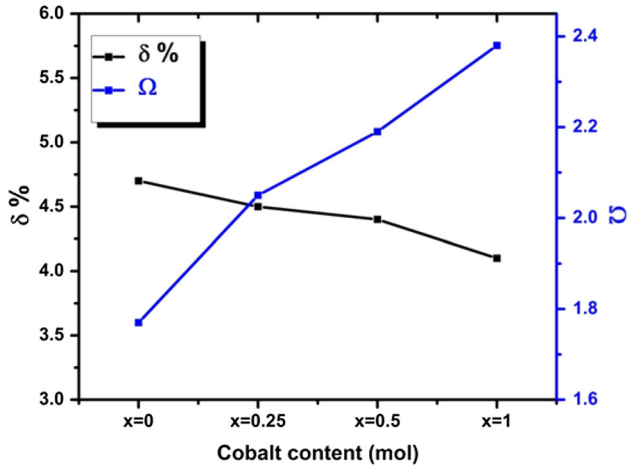

Fig. 10 Variation of δ% and Ω with cobalt content

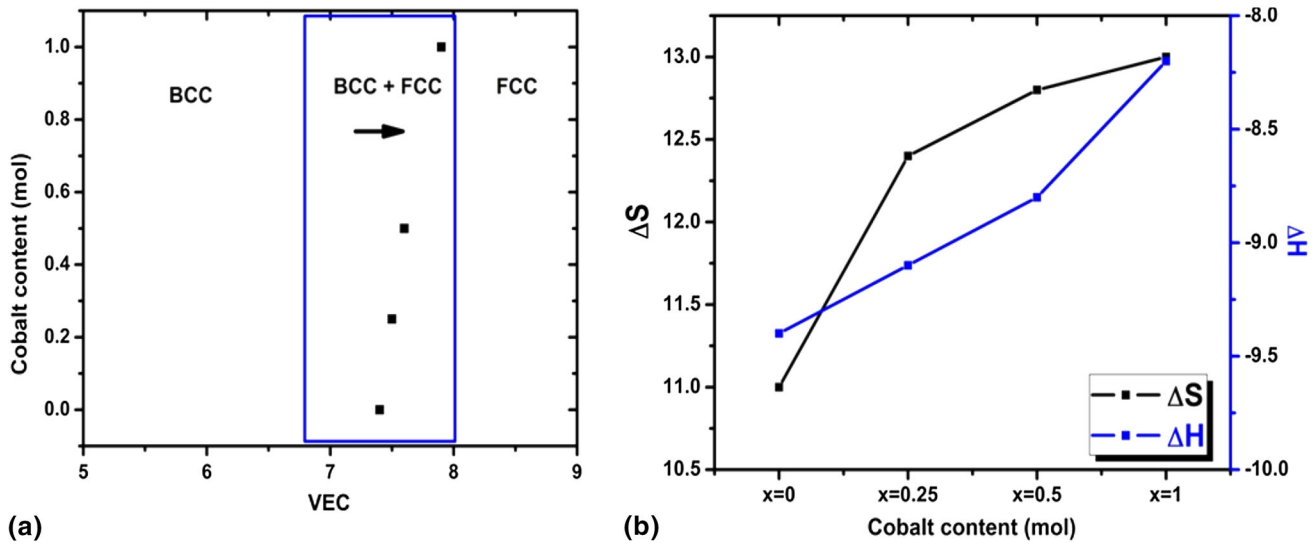

Fig. 9 Variation of (a) VEC and (b) enthalpy of mixing, and entropy of mixing with cobalt content from $x = 0$ to $x = 1.0$ mol

4. Conclusions

In the present study, $Al_{0.4}FeCrNiCo_x$ ($X = 0$, 0.25, 0.5, 1.0 mol) HEAs are successfully prepared by arc melting method from cold-compacted pellets. The XRD and SEM analyses indicate that the crystal structure of the as-cast Co = 0, Co = 0.25, and Co = 0.5 HEAs have mixed phases of FCC + BCC structure and the Co = 1 HEA has a single phase of FCC structure. The DSC analysis has indicated that up to 1000 °C there is no endothermic peak, and $Al_{0.4}FeCrNiCo_x$ ($x = 0$, 0.25, 0.5, 1.0 mol) HEAs are thermally stable up to 1000 °C. The thermal conductivity of the HEAs are observed to decrease from 4.87 W/mK to 2.674 W/mK, and the electrical resistivity is observed to vary from 150.30 to 273.74 μΩ-cm with the addition of cobalt from $x = 0$ to 1.0 mol. The compressive test of $Al_{0.4}FeCrNiCo_x$ ($x = 0$, 0.25, 0.5, 1.0 mol) HEAs indicates that the compressive yield strength decreases from 965.22 to 233.37 MPa, and the microhardness decreases from 253.6 to 155.6 HV. Thermodynamic parameters confirm that the $Al_{0.4}FeCrNiCo_x$ ($x = 0$, 0.25, 0.5, 1.0 mol) HEAs follow the theoretical condition of solid-solution formation.

Acknowledgments

Authors are thankful to the Institute (Malaviya National Institute of Technology, Jaipur) for financial support, Material Research Center, MNIT Jaipur, and ACMS, IIT Kanpur, for providing experimental facilities and Prof. Anandh Subramaniam (IIT Kanpur) for providing arc melting facility.

References

1. J.W. Yeh, S.K. Chen, S.J. Lin, J.Y. Gan, T.S. Chin, T.T. Shun, C.H. Tsau, and S.Y. Chang, Nanostructured High-Entropy Alloys with Multiple Principal Elements: Novel Alloy Design Concepts and Outcomes, *Adv. Eng. Mater.*, 2004, **6**(5), p 299–303
2. J.W. Yeh, Physical Metallurgy of High-Entropy Alloys, *JOM*, 2015, **67**(10), p 2254–2261
3. B.S. Murty, J.W. Yeh, and S. Ranganathan, High-Entropy Alloys, Butterworth-Heinemann, London, 2014, ISBN: 978-0-12-800251-3, pp. 1–204
4. D. Kumar, O. Maulik, S. Kumar, Y.V.S.S. Prasad, and V. Kumar, Phase and Thermal Study of Equiatomic AlCuCrFeMnW High Entropy Alloy Processed via Spark Plasma Sintering, *Mater. Chem. Phys.*, 2018, **210**, p 71–77
5. T.M. Butler and M.L. Weaver, Investigation of the Phase Stabilities in AlNiCoCrFe High Entropy Alloys, *J. Alloys Compd.*, 2017, **691**, p 119–129
6. A. Munitz, S. Salhov, S. Hayun, and N. Frage, Heat Treatment Impacts the Micro-Structure and Mechanical Properties of AlCoCrFeNi High Entropy Alloy, *J. Alloys Compd.*, 2016, **683**, p 221–230
7. T.T. Shun and Y.C. Du, Microstructure and Tensile Behaviors of FCC $Al_{0.3}CoCrFeNi$ High Entropy Alloy, *J. Alloys Compd.*, 2009, **479**(1-2), p 157–160
8. Y. Dong and Y. Lu, Effects of Tungsten Addition on the Microstructure and Mechanical Properties of Near-Eutectic $AlCoCrFeNi_2$ High-Entropy Alloy, *J. Mater. Eng. Perform.*, 2018, **27**(1), p 109–115
9. X. Hu and D. Chen, Effect of Ceramic Rolling and Annealing on Mechanical Properties of $AlCoCrFeNi_{2.1}$ Eutectic High-Entropy Alloys, *J. Mater. Eng. Perform.*, 2018, **27**(7), p 3566–3573
10. Z.M. Jiao, S.G. Ma, G.Z. Yuan, Z.H. Wang, H.J. Yang, and J.W. Qiao, Plastic Deformation of $Al_{0.3}CoCrFeNi$ and AlCoCrFeNi High-Entropy Alloys Under Nanoindentation, *J. Mater. Eng. Perform.*, 2015, **24**(8), p 3077–3083
11. L. Tian, Z.M. Jiao, G.Z. Yuan, S.G. Ma, Z.H. Wang, H.J. Yang, Y. Zhang, and J.W. Qiao, Effect of Strain Rate on Deformation Behavior of AlCoCrFeNi High-Entropy Alloy by Nanoindentation, *J. Mater. Eng. Perform.*, 2016, **25**(6), p 2255–2260
12. R. Wang, K. Zhang, C. Davies, and X. Wu, Evolution of Microstructure, Mechanical and Corrosion Properties of AlCoCrFeNi High-Entropy Alloy Prepared by Direct Laser Fabrication, *J. Alloys Compd.*, 2017, **694**, p 971–981
13. C.M. Lin and H.L. Tsai, Evolution of Microstructure, Hardness, and Corrosion Properties of High-Entropy $Al_{0.5}CoCrFeNi$ Alloy, *Intermetallics*, 2011, **19**(3), p 288–294
14. D. Kumar, O. Maulik, V.K. Sharma, Y.V.S.S. Prasad, and V. Kumar, Understanding the Effect of Tungsten on Corrosion Behavior of $AlCuCrFeMnW_x$ High-Entropy Alloys in 3.5 wt% NaCl Solution, *J. Mater. Eng. Perform.*, 2018, **27**(9), p 4481–4488
15. T.M. Butler and M.L. Weaver, Oxidation Behavior of Arc Melted AlCoCrFeNi Multi-Component High-Entropy Alloys, *J. Alloys Compd.*, 2016, **674**, p 229–244
16. Y.X. Liu, C.Q. Cheng, J.L. Shang, R. Wang, P. Li, and J. Zhao, Oxidation Behavior of High-Entropy Alloys AlxCoCrFeNi ($x = 0.15$, 0.4) in Supercritical Water and Comparison, *Trans. Nonferrous Met. Soc. China.*, 2015, **25**(4), p 1341–1351
17. N.K. Prasad and V. Kumar, Structure–Magnetic Properties Correlation in Mechanically Alloyed Nanocrystalline Fe–Co–Ni–(Mg–Si)x Alloy Powders, *J. Mater. Sci.: Mater. Electron.*, 2016, **27**(10), p 10136–10146
18. Y. Dong, L. Jiang, Z. Tang, Y. Lu, and T. Li, Effect of Electromagnetic Field on Microstructure and Properties of Bulk $AlCrFeNiMo_{0.2}$ High-Entropy Alloy, *J. Mater. Eng. Perform.*, 2015, **24**(11), p 4475–4481
19. Y. Wang, Y. Yang, H. Yang, M. Zhang, and J. Qiao, Effect of Nitriding on the Tribological Properties of $Al_{1.3}CoCuFeNi_2$ High-Entropy Alloy, *J. Alloys Compd.*, 2017, **725**, p 365–372
20. Y. Wang, Y. Yang, H. Yang, M. Zhang, and S. Ma, Microstructure and Wear Properties of Nitrided AlCoCrFeNi High-Entropy Alloy, *Mater. Chem. Phys.*, 2018, **210**, p 233–239
21. X. Ji, S.H. Alavi, S.P. Harimkar, and Y. Zhang, Sliding Wear of Spark Plasma Sintered CrFeCoNiCu High-Entropy Alloy Coatings: Effect of Aluminum Addition, *J. Mater. Eng. Perform.*, 2018, **27**(11), p 5815–5822
22. K. Lentzaris, A. Poulia, E. Georgatis, A.G. Lekatou, and A.E. Karantzalis, Analysis of Microstructure and Sliding Wear Behavior of $Co_{1.5}CrFeNi_{1.5}Ti_{0.5}$ High-Entropy Alloy, *J. Mater. Eng. Perform.*, 2018, **27**(10), p 5177–5186
23. M.X. Ren, B.S. Li, and H.Z. Fu, Formation Condition of Solid Solution Type High-Entropy Alloy, *Trans. Nonferrous Met. Soc. China*, 2013, **23**(4), p 991–995
24. Y. Zhang and W.J. Peng, Microstructural Control and Properties Optimization of High-Entropy Alloys, *Procedia Eng.*, 2012, **27**, p 1169–1178
25. S. Guo, C. Ng, J. Lu, and C.T. Liu, Effect of Valence Electron Concentration on Stability of fcc or bcc Phase in High Entropy Alloys, *J. Appl. Phys.*, 2011, **109**(10), p 103505
26. J.W. Qiao, S.G. Ma, E.W. Huang, C.P. Chuang, P.K. Liaw, and Y. Zhang, Microstructural Characteristics and Mechanical Behaviors of AlCoCrFeNi High-Entropy Alloys at Ambient and Cryogenic Temperature, *Mater. Sci. Forum*, 2011, **688**, p 419–425
27. J. Joseph, T. Jarvis, X. Wu, N. Stanford, P. Hodgson, and D.M. Fabijanic, Comparative Study of the Microstructures and Mechanical Properties of Direct Laser Fabricated and Arc-Melted $Al_xCoCrFeNi$ High Entropy Alloys, *Mater. Sci. Eng. A*, 2015, **633**, p 184–193
28. S. Niu, H. Kou, T. Guo, Y. Zhang, J. Wang, and J. Li, Strengthening of Nano Precipitations in an Annealed $Al_{0.5}CoCrFeNi$ High Entropy Alloy, *Mater. Sci. Eng. A*, 2016, **671**, p 82–86
29. Z. Wang, M.C. Gao, S.G. Ma, H.J. Yang, Z.H. Wang, M.Z. Moroz, and J.W. Qiao, Effect of Cold Rolling on the Microstructure and Mechanical Properties of $Al_{0.25}CoCrFe_{1.25}$ $Ni_{1.25}$ High-entropy alloy, *Mater. Sci. Eng. A.*, 2015, **645**, p 163–169
30. Y.F. Kao, T.J. Chen, S.K. Chen, and J.W. Yeh, Microstructure and Mechanical Property of as-Cast, -Homogenized, and -Deformed $Al_xCoCrFeNi$ ($0 \le x \le 2$) High-Entropy Alloys, *J. Alloys Compd.*, 2009, **488**(1), p 57–64
31. I.S. Wani, T. Bhattacharjee, S. Sheikh, P.P. Bhattacharjee, S. Guo, and N. Tsuji, Tailoring Nanostructures and Mechanical Properties of $AlCoCrFeNi_{2.1}$ Eutectic High Entropy Alloy Using Thermo-Mechanical Processing, *Mater. Sci. Eng. A*, 2016, **675**, p 99–109

32. W. Chen, Z. Fu, S. Fang, H. Xiao, and D. Zhu, Alloying Behavior, Microstructure and Mechanical Properties in a $FeNiCrCo_{0.3}Al_{0.7}$ High Entropy Alloy, *Mater. Des.*, 2013, **51**, p 854–860
33. S. Fang, W. Chen, and Z. Fu, Microstructure and Mechanical Properties of Twinned $Al_{0.5}CrFeNiCo_{0.3}C_{0.2}$ High Entropy Alloy Processed by Mechanical Alloying and Spark Plasma Sintering, *Mater. Des.*, 2014, **54**, p 973–979
34. Y. Zhao, H. Cui, M. Wang, Y. Zhao, X. Zhang, and C. Wang, The Microstructures and Properties Changes Induced by Al: Co Ratios of the $Al_xCrCo_{2-x}FeNi$ High Entropy Alloys, *Mater. Sci. Eng. A*, 2018, **733**, p 153–163
35. G. Qin, W. Xue, C. Fan, R. Chen, L. Wang, Y. Su, H. Ding, and J. Guo, Effect of Co Content on Phase Formation and Mechanical Properties of $(AlCoCrFeNi)_{100-x}Co_x$ High-Entropy Alloys, *Mater. Sci. Eng. A*, 2018, **710**, p 200–205
36. K. Jasiewicz, J. Cieslak, S. Kaprzyk, and J. Tobola, Relative Crystal Stability of $Al_xFeNiCrCo$ High Entropy Alloys from XRD Analysis and Formation Energy Calculation, *J. Alloys Compd.*, 2015, **648**, p 307–312
37. Y. Dong, X. Gao, Y. Lu, T. Wang, and T. Li, A Multi-Component $AlCrFe2Ni_2$ Alloy with Excellent Mechanical Properties, *Mater. Lett.*, 2016, **169**, p 62–64
38. J. Wang, T. Guo, J. Li, W. Jia, and H. Kou, Microstructure and Mechanical Properties of Non-Equilibrium Solidified CoCrFeNi High Entropy Alloy, *Mater. Chem. Phys.*, 2018, **210**, p 192–196
39. H.P. Chou, Y.S. Chang, S.K. Chen, and J.W. Yeh, Microstructure, Thermophysical and Electrical Properties in $Al_xCoCrFeNi$ ($0 \le x \le 2$) High-Entropy Alloys, *Mater. Sci. Eng. B*, 2009, **163**(3), p 184–189
40. S. Uporov, V. Bykov, S. Pryanichnikov, A. Shubin, and N. Uporova, Effect of Synthesis Route on Structure and Properties of AlCoCrFeNi High-Entropy Alloy, *Intermetallics*, 2017, **83**, p 1–8
41. B. Cantor, I.T.H. Chang, P. Knight, and A.J.B. Vincent, Microstructural Development in Equiatomic Multicomponent Alloys, *Mater. Sci. Eng. A*, 2004, **375–377**, p 213–218
42. S. Guo and C.T. Liu, Phase Stability in High Entropy Alloys Formation of Solid-Solution Phase or Amorphous Phase, *Prog. Nat. Sci. Mater. Int.*, 2011, **21**(6), p 433–446
43. Y. Zhang, T.T. Zuo, Z. Tang, M.C. Gao, K.A. Dahmen, P.K. Liaw, and Z.P. Lu, Microstructures, and Properties of High-Entropy Alloys, *Prog. Mater Sci.*, 2014, **61**, p 1–93
44. S. Guo, Phase Selection Rules for Cast High Entropy Alloys: An Overview, *Mater. Sci. Technol.*, 2015, **31**(10), p 1223–1230
45. W. Martienssen and H. Warlimont, *Handbook of Condensed Matter and Materials Data*, Springer, Berlin, 2005, ISBN 3-540-44376-2
46. Y. Dong, Y. Lu, L. Jiang, T. Wang, and T. Li, Effects of Electro-Negativity on the Stability of Topologically Close Packed Phase in High Entropy Alloys, *Intermetallics*, 2014, **52**, p 105–109

Publisher's Note Springer Nature remains neutral with regard to jurisdictional claims in published maps and institutional affiliations.